HEFAT2007
5th International Conference on Heat Transfer, Fluid Mechanics and Thermodynamics
Sun City, South Africa
Paper number: CM4

FLOW PATTERN-BASED HEAT TRANSFER CORRELATION FOR CONDENSING R-22 IN A SMOOTH TUBE

Christians-Lupi M., van Rooyen E., Liebenberg L. and Meyer J.P.*
*Author for correspondence
Department of Mechanical and Aeronautical Engineering,
University of Pretoria,
Pretoria, 0002,
South Africa,
E-mail: jmeyer@up.ac.za

ABSTRACT

This paper presents a study of probabilistic flow regime-based heat transfer coefficients during refrigerant condensation inside a smooth tube. Experimental work was conducted using refrigerant R-22, at an average saturation temperature of 40°C, with mass fluxes ranging from 250-650 kg/m^{2}s, and with test section inlet vapor qualities ranging from 0.65 down to 0.10. These tests conditions represent mostly Intermittent flow, with some data points in the Annular and Stratified-wavy flow regimes. Utilizing time fraction data gathered in this experimental setup, a new time fraction-corrected flow regime-based heat transfer correlation, heavily based on the Thome *et al.* (J.R. Thome, J. El Hajal and A. Cavallini, Condensation in horizontal tubes, part 2: New heat transfer model based on flow regimes, International Journal of Heat and Mass Transfer, 46:3365-3387, 2003) correlation was developed for use in the Intermittent flow regime. The modified correlation predicted the experimental data with a mean absolute deviation of 10%.

INTRODUCTION

FLOW PATTERN MAPS

Kattan *et al.* [1-4] proposed the first flow-boiling model for evaporation inside horizontal tubes based on the local flow pattern and a newly developed diabatic flow pattern map, to predict two-phase flow regime transitions. El Hajal *et al.* [5] adapted the flow-boiling two-phase flow pattern map, originally developed by Kattan *et al.* for condensation inside horizontal tubes. Furthermore, due to the very high reduced pressures found in condensation and the sensitivity of regime transitions, heat transfer and pressure drop to void fraction, they defined a new log-mean void fraction model, capable of predicting the void fraction accurately for low (atmospheric) to very high reduced pressures (near critical pressure) [5,6]. El Hajal *et al.* [5] simplified the implementation of the map by substituting the iterative calculation of the stratification angle with a direct calculation method [7]. Also, the changes proposed by Zürcher *et al.* [8] were implemented to ensure better prediction of the transition curves from annular to stratified/wavy flow, and from stratified/wavy to wavy flow. The Thome flow map is shown in Fig. 1.

NOMENCLATURE

Symbol	Description
A	area (m^2)
d	diameter (m)
EB	energy balance (%)
G	mass flux (kg m^{-1}s^{-1})
g	gravitational acceleration (m s^{-2})
h	enthalpy (J kg^{-1})
h	heat transfer coefficient (W m^{-2}K^{-1})
k	thermal conductivity (W m^{-1}K^{-1})
L	length of test section (m)
$\dot{m}$	mass flow (kg s^{-1})
p	pressure (Pa)
$\dot{Q}$	heat transferred (W)
Re	Reynolds number
R_w	wall thermal resistance (W^{-1}m K)
T	temperature (°C)
tf	time fraction
x	vapor quality / thermocouple position (m)
Greek Symbols	
θ	falling film angle (rad)
Subscripts	
b	bulk
Cu	copper
c	convective
exp	experimental
$grav$	gravity-dominated
H_2O	water
i	inner/inlet
IA	Intermittent-Annular transition
L	liquid/length
o	outer
ref	refrigerant
sat	saturation
$shear$	shear stress-dominated
$strat$	stratified
tf	time fraction
V	vapor
w	wall
$wavy$	Intermittent-wavy transition

TIME FRACTION

At present, two main methods of forced heat transfer in condensing two-phase flow in horizontal tubes have been identified, namely gravity-dominated and shear-stress dominated heat transfer (Collier and Thome [6] Liebenberg [9]). However, neither one of these can

adequately describe the heat transfer in the Intermittent flow regime, as defined by Thome *et al.* [5]. Only taking still pictures of flow condensing in the Intermittent flow regime can lead to erroneous conclusions regarding the flow. A still image can be taken as a slug goes across the camera, and by only analyzing this freeze-frame (even if other 'objective' methods are used), it might be thought that there is only Stratified flow; however, over time, looking at the other stills before and after, including other objectively analyzed data, it might be discernible that a slug was traveling past the camera.

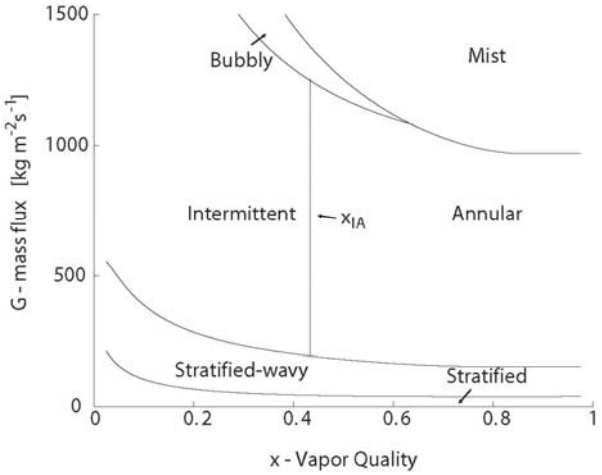

Fig. 1: Thome flow map for R-134a condensing in an 8.11 mm ID tube at a nominal saturation temperature of 40°C.

From a heat transfer perspective, this temporal variability in the flow has a large effect that has not yet been quantified. Furthermore, a simple shear-controlled model (*i.e.* Annular flow) or a gravity-controlled model will not suffice on their own. Thus, we can clearly distinguish that in a single flow regime, the two separate heat transfer modes will have an effect. So the main question now is: if analysis is carried out to find out what the probability is that at a certain vapor quality and mass flux one or the other heat transfer mode will dominate, can a more accurate method of predicting heat transfer be developed?

EXPERIMENTAL FACILITY

The experimental test facility consisted of two main sub-systems: the vapor-compression loop, and the water cycles. Each of the sub-systems was of the closed-cycle type. The experimental test facility can be utilized for both condensation and evaporation tests. Steady state conditions were assumed when the energy balance error (EB) was less than 1%, and the temperatures and pressures of the system were constant for a period of at least 10 minutes. Further, experimental conditions were also maintained such that the vapor quality difference over the test section was less than 10% (5% is ideal). A schematic of the layout of the system is given in Fig. 2.

The test section was constructed of a 9.53 mm outer diameter copper tube. At the entrance of the test line, a straight calming section, 50 tube diameters long was utilized

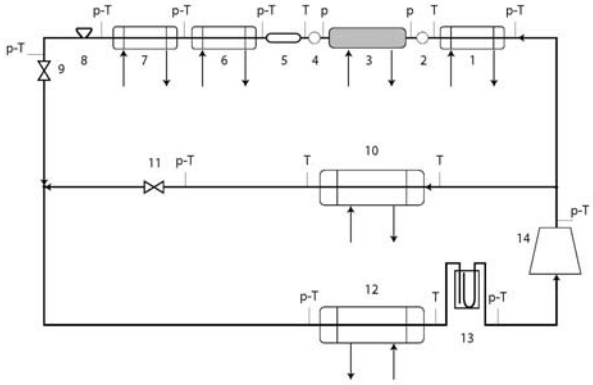

1. Pre-condenser (water cooled)
2. Sight glass: high-speed videography
3. Test section (water cooled)
4. Sight glass
5. Capacitive void fraction sensor
6. Post-condenser (water cooled)
7. Sub-cooler (water cooled)
8. Coriolis mass flow meter
9. Test line expansion valve
10. Bypass condenser (water cooled)
11. Bypass line expansion valve
12. Evaporator (water cooled)
13. Suction Accumulator
14. Compressor

Fig. 2: Test setup schematic [10]. The arrows indicate flow direction.

to make sure the flow was developed [11]. A cylindrical sight glass was installed at the inlet of the test heat exchanger, and was used to analyze the flow using spectral methods, with a high-speed video camera. The inner tube outer wall temperatures of the 1.5 m long test section were measured at seven stations using four type-T thermocouples per station. A second sight glass was installed at the exit of the test section. These sight glasses were used not only for flow visualization purposes, but also as insulators against thermal axial conduction in the copper tube. The inlet and outlet temperatures of the inner tube were measured before the inlet and after the outlet sight glasses.

The absolute pressures of the condensing refrigerant were measured using piezoelectric pressure transducers, which were positioned at the inlet and outlet of the test section, between the sight glasses. The refrigerant and water mass flows were measured using Coriolis mass flow meters. The oil concentration in the refrigerant was measured using ASHRAE Standard 41.4 [12], and was calculated as 2.3%.

DATA REDUCTION

The properties of the refrigerant at the inlet of the pre-condenser and outlet of the post-condenser were determined by temperature and pressure measurements. From these measurements, the thermo-physical properties of the condensing refrigerant were determined by utilizing data from a refrigerant property database [13] and a program called XProps [14].

Due to the fact that it is not possible to measure the heat transferred out of the refrigerant line over the test section directly, an energy balance error of less than 1% must be obtained before the water-side heat transfer is utilized to calculate the outlet refrigerant properties. This same principle is also valid for the pre-condenser. The average inlet and outlet vapor qualities are obtained using:

$$x_j = \frac{h_j - h_{L,j}}{h_{V,j} - h_{L,j}} \qquad (1)$$

In the above, *j* is utilized to denote either the inlet or outlet of the test section. *L* and V denote the saturated liquid and vapor enthalpy values at T_j. The values of the enthalpy were calculated using

$$h_j = h_k - \left| \frac{\dot{Q}_{kj}}{\dot{m}_{ref}} \right| \quad (2)$$

In the above equation, *k* denotes the position prior to position *j*; that is, if calculating the test inlet vapor quality, *k* denotes the pre-condenser refrigerant inlet, while if the test outlet vapor quality is calculated, *k* denotes the inlet of the test section. The average vapor quality of the test section is determined by the arithmetic mean of the inlet and outlet calculated vapor qualities.

Then, the heat transfer coefficient is calculated using the mean wall temperature of the test section, the heat transferred into the water-side of the test section, and the mean refrigerant temperature between the inlet and the outlet. The wall temperature average is found by using the physical distance between station and the Trapezium numerical integration method, ensuring that any non-linearity in temperature distribution over the length of the tube wall can be reflected in a more representative average.

The inner wall temperature, such that the proper temperature difference may be calculated, is

$$T_{w,i}^{j} = T_{w,o}^{j} + \left| \dot{Q}_{H_2O} R_w \right| \quad (3)$$

Where R_w is the wall thermal resistance, and is

$$R_w = \frac{\ln \frac{d_{i,o}}{d_{i,i}}}{2\pi k_{Cu} L} \quad (4)$$

And $d_{i,o}$ and $d_{i,i}$ are the outer and inner diameters of the inner tube, k_{Cu} is the thermal conductivity of copper (calculated as a function of temperature [15]) and *L* is the length of the test section. Then, the semi-local experimental heat transfer coefficient is

$$h_{c,\exp} = \left| \frac{\dot{Q}_{H_2O}}{A_L (\bar{T}_{w,i} - \bar{T}_b)} \right| \quad (5)$$

FLOW REGIME OBSERVATIONS AND THE EFFECT OF TIME FRACTION

In this study, the time fraction map for the Intermittent flow regime varies as a function of mass flux and quality between two absolute values, 0 and 1, which describe fully gravity-dominated and shear stress-dominated flows respectively. In this work, the time fraction number, *tf*, has been defined for this purpose. The objective method of data analysis required for this data was developed in parallel by Van Rooyen [16], in which the high-speed videography data captured during testing was used in conjunction with measured dynamic void fraction (from the capacitive sensor) and pressure transducer data used to obtain discrete measurements of this time fraction over a range of mass flux and vapor quality. The time fraction data is overlaid on the Thome flow map in Fig. 3. It should be noted that the time fraction data is not parameterized. This is due to the fact that data were only captured with one refrigerant (R-22) and one tube diameter (8.38 mm ID). To parameterize this data, data are needed in which different tube diameters are used, with a wider variety of refrigerants, such that the physical characteristics are captured.

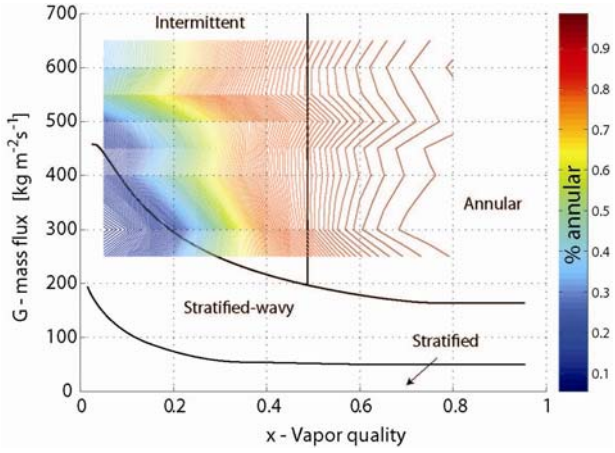

Fig. 3: Time fraction data [16] overlaid on the Thome map [5,7] for condensing R-22 in an 8.38 mm ID tube, at a nominal saturation temperature of 40°C.

TIME FRACTION-CORRECTED HEAT TRANSFER CORRELATION

The ability to determine the probability that, at a certain mass flow and vapor quality, a certain heat transfer mode will prevail can directly aid us in increasing the accuracy of existing heat transfer correlations, not by changing the leading coefficients and exponents for ones that better fit our experimental data, but by directly modeling the physics of the flow. The time fraction map, primarily developed by Van Rooyen [16], is based on one single, fundamental assumption. This assumption is that, at every single point in the time fraction map (*i.e.* at distinct combinations of mass flux and vapor quality), the heat transfer dominance is shifted from gravity-based to shear stress-based in a linear fashion. This is to say that if *tf* fraction of the time is spent in shear stress-dominated heat transfer mode, then (*1-tf*) will be spent in the gravity-dominated heat transfer mode. From the above, we can begin by postulating that the time fraction corrected heat transfer coefficient in the Intermittent flow regime would be a linear combination of the shear stress- and gravity-based heat transfer coefficients, in the form

$$h_{c,tf} = tf \cdot h_{c,shear} + (1 - tf) \cdot h_{c,grav} \quad (6)$$

where $h_{c,shear}$ and $h_{c,grav}$ are calculated from the Thome *et al.* [7] correlation. The only change performed to Thome's correlation is a small modification of the falling film angle θ, shown below.

$$\theta = \theta_{strat} \left[\frac{G_{wavy} - G}{G_{wavy} - G_{strat}} \right]^{0.5} \quad (7)$$

The term in square brackets is a multiplier that can vary between 0 and 1, in the limiting cases of the mass flux being equal to the transition values between Stratified and Stratified-Wavy (G_{strat}) and the transition value between Stratified-Wavy and Intermittent (G_{wavy}). The purpose of the multiplier is to change the value of the stratification angle smoothly from its highest value, θ_{strat}, at the interface between Stratified and Stratified-Wavy down to 0, at the interface with Intermittent. However, we are interested in finding the stratification angle for times in which the mass flux is larger than the Wavy transition. Attempting this with the multiplier gives a complex number, due to the fact that it is square-rooted (and the top subtraction will always generate a negative number). The proposed change that is performed to this term is to make the multiplier a constant value of 1. This is to say that the falling film angle θ is made equal to the stratification angle θ_{strat}.

In the analysis of the Intermittent flow regime visual data, it was found that the periods classified as gravity-dominated (Stratified) actually had very small to no waves present, thus allowing us to assume that the stratification angle was that of the completely Stratified flow regime.

EXPERIMENTAL HEAT TRANSFER COEFFICIENT RESULTS

Utilizing the smooth test-section as described above, and R-22 as the test refrigerant, a total of 101 data points were captured, ranging in mass flux from 250 kg/m^{2}s up to 650 kg/m^{2}s, and with a vapor quality varying between 0.05 and 0.65. When developing the test matrix, it was required that some data points fall into what Thome defines as the stratified-wavy regime and the annular flow regime, such that the time-fractional analysis could be performed including flow regime transitions. The mean testing information for the data points is summarized in Table 1.

Table 1: R-22 condensation experimental summary

Measurand	Mean	Standard deviation
T_{sat}	39.7 ^{o}C	±1.9 ^{o}C
p_{sat}	1449 kPa	±65 kPa
EB	0.65%	±0.26%
$\dot{m}_{ref}$	Test dependent	max: ± 2 kg/m^{2}s

Fig. 4 presents the experimental heat transfer coefficient against the Thome heat transfer coefficient. The values for the Thome heat transfer coefficient were calculated utilizing the required heat transfer coefficient form, depending on the flow regime in which the data point was situated. The mean percentage deviation of the experimental heat transfer coefficient with respect to the Thome heat transfer coefficient is, on average, 13%.

Carrying on with the analysis, the time fraction corrected heat transfer coefficient was calculated. Fig. 5 shows the experimental heat transfer coefficient plotted against both the time fraction-corrected and (classical) Thome heat transfer coefficient correlation. The experimental results' mean percentage deviation when compared against the time fraction-corrected heat transfer correlation is 10%. Analyzing the data in Fig. 5, it can be shown that the points that were at the lower range of both mass flux (250-300 kg/m^{2}s) and vapor quality, which were both underpredicted by the (classical) Thome correlation are now within ±25% of the predicted value.

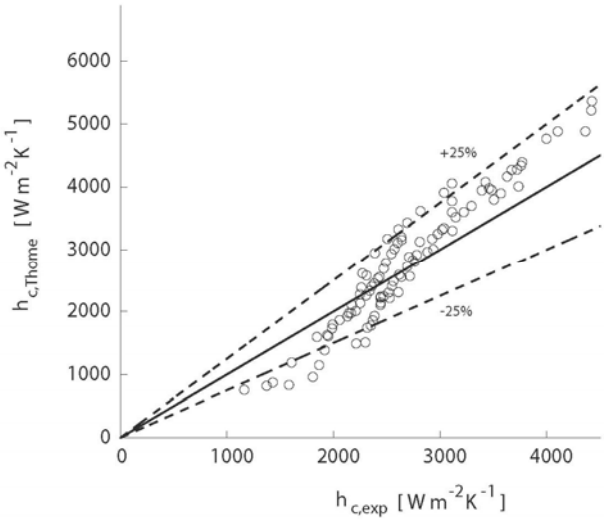

Fig. 4: Experimental heat transfer results comparison to Thome's correlation at mass fluxes between 250 and 650 kg/m^{2}s

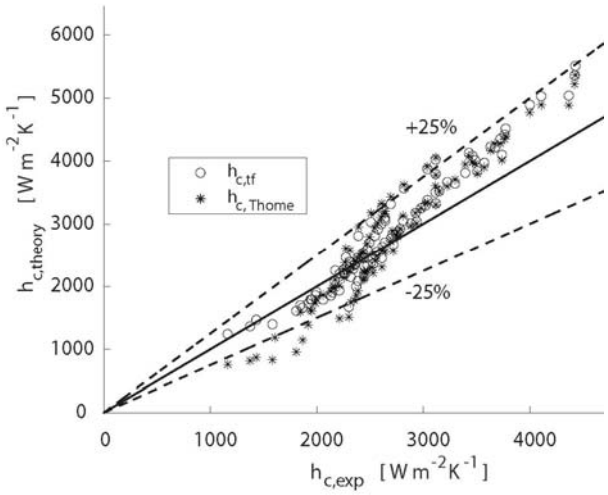

Fig. 5: Comparison of experimental heat transfer coefficient against the time fraction-corrected heat transfer prediction at mass fluxes between 250 and 650 kg/m^{2}s.

Fig. 6 shows the experimental heat transfer coefficients compared to both the time fraction corrected heat transfer and the (classical) Thome correlation for a constant mass flux of 250 kg/m^{2}s. The mean percentage deviation between the time fraction corrected heat transfer coefficients and the experimental results drop to 10%. In contrast, for the same mass flux, the experimental results' mean deviation from the Thome heat transfer coefficient predictions is 27.6%.

On a point-by-point direct comparison between the prediction of the time fraction-corrected model and the

Thome prediction, it can be seen that the points at lower vapor qualities benefited the most from the application of the time fraction data. As the vapor quality increases, and the heat transfer coefficient increases (since the flow regime tends towards the Annular flow regime), the influence of the time fraction is lessened; this is mainly for two reasons, the first being that the *tf* is large, which makes the influence of the shear stress-based heat transfer coefficient more apparent, and secondly, at higher vapor qualities (and mass fluxes), the shear stress-based heat transfer coefficient becomes dominant, as shown in Fig. 7.

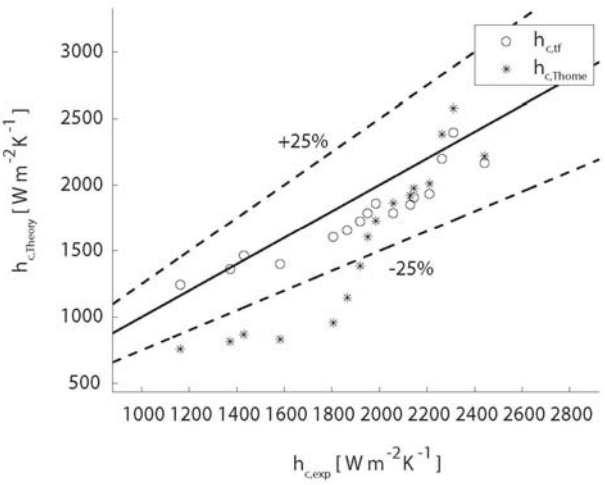

Fig. 6: Comparison of the experimental heat transfer coefficients against predicted data at G = 250 kg/m^{2}s

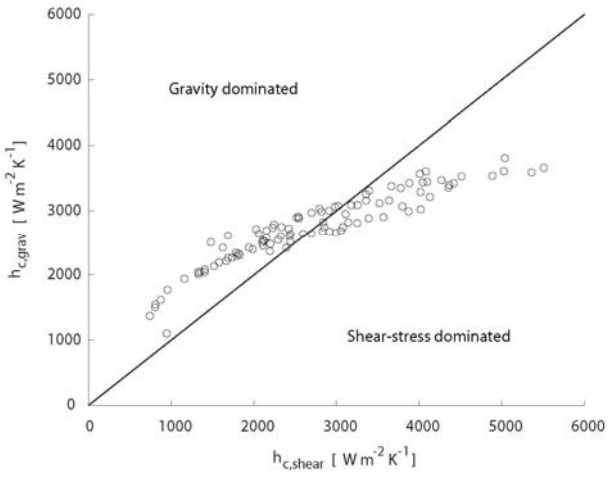

Fig. 7: Comparison of shear stress-based and gravity-based coefficient dominance

Due to their proximity to the Stratified-Wavy/Intermittent Thome transition curve, the data points at the lowest vapor qualities (at G = 250 kg/m^{2}s) experience a large variation in heat transfer mode dominance, which is not captured well by the existing active Thome correlation. As the vapor quality increases, the heat transfer prediction tends towards the shear stress-based heat transfer coefficient prediction, which is expected from the form of the time fraction-corrected heat transfer correlation. The data found at a mass flux of 300 kg/m^{2}s also continues the trends found in the data presented in Fig. 6.

The data found at 350 and 400 kg/m^{2}s is presented in Fig. 8. The heat transfer coefficients at the lower qualities show the best improvement, as has been the trend up to now. At these mass fluxes, the shear stress and gravity heat transfer coefficients values, as depicted in Fig. 7, are very close to each other, which is why the time fraction corrected points do not vary very much from their Thome counterparts.

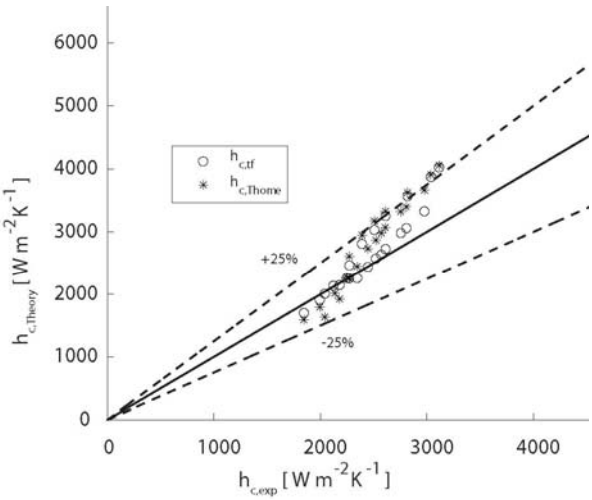

Fig. 8: Comparison of the experimental heat transfer coefficients against predicted data at G = 350-400 kg/m^{2}s

Starting at mass fluxes higher than 450 kg/m^{2}s, the time fraction goes to high levels faster than at lower mass fluxes, which means that number of data points that are heavily affected by the time fraction correction decrease. Case in point, at G=450 kg/m^{2}s, half of the data points are very near their Thome counterparts, all of these at the higher vapor qualities, while the meaningful prediction corrections are still effected at lower vapor qualities. Furthermore, at vapor qualities still in the Intermittent flow but not close to the Intermittent/Annular transition curve, the influence of the gravity term is attenuated, generating results similar to those found with the Thome correlation at these high mass fluxes. Fig. 9 shows data gathered at mass fluxes between 450 and 550 kg/m^{2}s.

At the mass fluxes between 600 and 650 kg/m^{2}s, the same trends as shown in Fig. 9 were found. Apart from the fact that the time fraction can be seen to rise more quickly, as evidenced in Fig. 3, on closer inspection of Fig. 7, at the range of heat transfer coefficients encountered at these higher mass flow rates (in relation to the rest of the test matrix), it can be seen that the shear stress-based prediction is quite higher than the gravity-based coefficient. This, coupled with the reduced influence of the time fraction (since it is large for a majority of vapor qualities in the Intermittent regime) ends up with a heat transfer coefficient prediction similar to the Thome correlation.

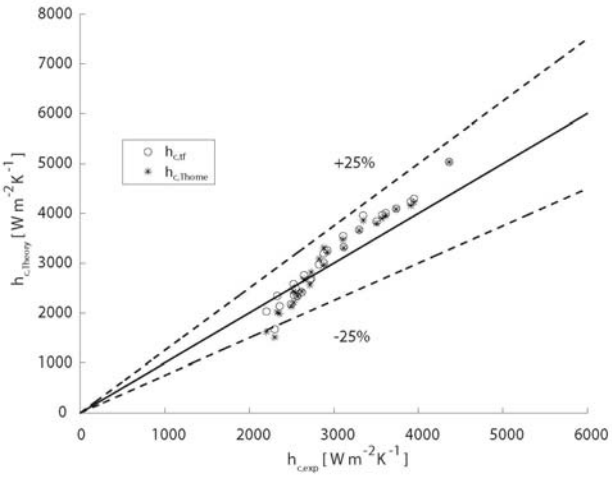

Fig. 9: Comparison of the experimental heat transfer coefficients against predicted data at G = 450-550 kg/m^{2}s

CONCLUSION

For the condensation experiments one smooth tube was tested utilizing refrigerant R-22 at a saturation temperature of 40^{o}C and at mass fluxes ranging from 250 to 650 kg/m^{2}s. Testing was performed mostly in the Intermittent flow regime.

From a time fraction point of view, the Intermittent flow regime was mapped in terms of two separate dominating heat transfer modes, those being shear stress- and gravity-based, of which mathematical models, exist. The time fraction was combined with the two flow regime-based correlations to create a time fraction-corrected flow pattern-based heat transfer correlation for the Intermittent flow regime, in an effort to better predict the heat transfer behavior in this regime.

Results showed that the new correlation predicted the data on average to a mean absolute deviation of 10%. It was shown that the time fraction correction has more effect when the vapor quality is low, and especially so when the mass flux is also relatively low (near the transition between Stratified-wavy and Intermittent, thus G = 250 kg/m^{2}s). This method improves the accuracy of the heat transfer coefficient predictions using an approach that models the governing physics of the Intermittent flow regime, rather than utilize a non-physical multiplier.

REFERENCES

[1] Kattan N, Thome JR, Favrat D. Measurement and prediction of two-phase flow patterns for new refrigerants inside horizontal tubes. ASHRAE Transactions 1995; 101(2)1251-57.

[2] Kattan N, Thome JR, Favrat D. Boiling of R-134a and R-123 in a microfin tube. Proc. 19th Int. Congr. of Refrigeration 1995; The Hague, Netherlands. 337-44.

[3] Kattan N, Thome JR, Favrat D. Flow boiling in horizontal tubes. Part 1: Development of a diabatic two-phase flow pattern map. Journal of Heat Transfer 1998; 120(1)140-47.

[4] Kattan N, Thome JR, Favrat D. Flow boiling in horizontal tubes. Part3: Development of a new heat transfer model based on flow patterns. Journal of Heat Transfer 1998; 120(1)156-65.

[5] El Hajal J, Thome JR, Cavallini A. Condensation in horizontal tubes, Part 1: Two-phase flow pattern map. International Journal of Heat and Mass Transfer 2003; 46:3349-63.

[6] Collier JG, Thome JR. Convective boiling and condensation, Clarendon Press, Oxford, 1994.

[7] Thome JR, El Hajal J. and Cavallini A. Condensation in horizontal tubes, Part 2: New heat transfer model based on flow regimes, International Journal of Heat and mass Transfer, 2003, 46:3365-3387.

[8] Zürcher O, Thome JR, Favrat D. Evaporation of ammonia in a smooth horizontal tube: heat transfer measurements and predictions. Journal of Heat Transfer 1998; 121:89-101.

[9] Liebenberg L., Thome J.R. and Meyer J.P., Flow visualization and flow pattern identification with power spectral density distributions of pressure traces during refrigerant condensation in smooth and microfin tubes, Journal of Heat Transfer, 2005, 127:209-220.

[10] Christians-Lupi M., Flow pattern-based heat transfer and pressure drop correlations for condensing refrigerants in smooth tubes, M.Eng. dissertation, University of Pretoria, 2007.

[11] Cho K., and Tae S.-J., Condensation heat transfer for R-22 and R-407C refrigerant-oil mixtures in a microfin tube with a U-bend, International Journal of Heat and Mass Transfer 2001; 44;2043–2051.

[12] ASHRAE, ASHRAE Standard 41.4: Method for measurement of proportion of lubricant in liquid refrigerant, 2006.

[13] REFPROP, NIST thermodynamic properties of refrigerants and refrigerant mixtures (REFPROP), Version 8.0, NIST Standard Reference Database 23, National Institute of Standards and Technology, Gaithersburg, MD, 2005.

[14] Xprops, Thermal Analysis Partners, University of Maryland, MD, http://www.thermalanalysispartners.com, 2006.

[15] Abu-Eishah S.I., Correlations for the thermal conductivity of metals as a function of temperature, International Journal of Thermophysics, 2001, 22:1855-1868.

[16] Van Rooyen E., Time-fractional Analysis of Flow Patterns during Refrigerant Condensation, M.Eng. dissertation, University of Pretoria, 2007.